Chinese Journal of
POLYMER SCIENCE

RESEARCH ARTICLE

https://doi.org/10.1007/s10118-023-2912-8
Chinese J. Polym. Sci. **2023**, *41*, 1386–1391

Conformation of an Amphiphilic Comb-like Copolymer in a Selective Solvent

Peng Hao[a,†], Xing-Hong Mai[a,†], Qiao-Yue Chen[a], and Ming-Ming Ding[a,b*]

[a] *Xinjiang Laboratory of Phase Transitions and Microstructures in Condensed Matter Physics, College of Physical Science and Technology, Yili Normal University, Yining 835000, China*
[b] *School of Chemical Engineering and Light Industry, Guangdong University of Technology, Guangzhou 510006, China*

Electronic Supplementary Information

Abstract We study the conformation of an amphiphilic comb-like copolymer in a selective solvent by using Brownian dynamics simulations. Our results demonstrate that, there is an optimal total degree of polymerization to form spherical micelles. Only when the total degree of polymerization is less than the optimal total degree of polymerization, a unimolecular spherical micelle can be formed, otherwise, the spherical micelle will be transformed into a cylindrical micelle. When the total degree of polymerization is less than the optimal total degree of polymerization, the radius of gyration and the stretching factor meet an exponential relationship, where the power exponent decreases with the increase of the length of hydrophilic side chains. The fundamental principles uncovered here afford insights for the optimization of molecular design of amphiphilic comb-like copolymers in various applications.

Keywords Comb-like copolymer; Conformation; Selective solvent; Brownian dynamics

Citation: Hao, P.; Mai, X. H.; Chen, Q. Y.; Ding, M. M. Conformation of an amphiphilic comb-like copolymer in a selective solvent. *Chinese J. Polym. Sci.* **2023**, *41*, 1386–1391.

Comb-like polymers are branched polymers consisting of polymeric side chains anchored to a linear backbone, different from linear homologues, they offer many unique physical and chemical properties,[1–7] which enable various potential applications such as templates of well-defined nanostructures, drug carriers, surfactants, and stimuli-responsive materials.[8–17]

In theory, Fredrickson,[18] Borisov,[19,20] Schmidt,[21] Dobrynin,[22] Sing,[23,24] and Lodge,[25] *et al*. have successively made significant contributions in modeling the conformational characteristics of comb-like chains in solution or melt, to name but a few. Due to advantages in simulations, numerous works have investigated the relationship between the microscopic conformational details of comb-like chains and molecular parameters from the molecular level, including Yethiraj,[26] Hsu and Binder,[27,28] Chatterjee,[29] Sing,[30,31] Deshmukh,[32] and Schroeder,[33–35] *et al*., to name but a few. Experimentally, Lodge *et al*. demonstrated that for the smaller grafting density, the effect of graft-graft excluded-volume interaction on the dimensions of comb-like chain can be ignored, which is consistent with the discussions from the Flory approximation.[25,36] Conversely, the experimental results of Li *et al*. did not support this view, and suggested that the graft-graft excluded-volume of side chains is important for the overall conformation.[37–39] Recently, using simulations, we found that the dimension of comb-like chains and the stretching factor satisfy a quantitative exponential relationship, which effectively validates the different experimental results.[40]

For the vast majority of comb-like polymers, the backbone and the side chains are often obtained from different monomers, including the experiments mentioned above,[25,36–39] which results in the backbone and the side chains being sensitive to the environmental factors such as temperature and solvent properties show different characteristics.[6] Among them, the amphiphilic comb-like copolymers in which the backbone is hydrophobic and the side chains are hydrophilic are particularly common. For example, Wang *et al*. prepared an amphiphilic biodegradable copolymer with hydrophobic poly(ε-caprolactone) grafted onto a short and water-soluble maltoheptaose backbone, which produces the wire-like micelles.[41] Kang *et al*. succeeded in synthesizing amphiphilic comb-like copolymers possessing a fluorescent hydrophobic P(NVK-*co*-VBC) backbone and pH-sensitive hydrophilic P(DMAEMA-*co*-AAc) side chains, which self-assembles into onion-like multilamellar vesicles in aqueous media.[11] Sheng *et al*. and Liu *et al*. studied the structural characteristics and fusion pathways of onion-like vesicles formed by

* Corresponding author, E-mail: mmding@gdut.edu.cn
† These authors contributed equally to this work.
Special Issue: Theory and Simulation of Macromolecules
Received October 15, 2022; Accepted November 25, 2022; Published online February 1, 2023

amphiphilic comb-like copolymers using dissipative particle dynamics,[42,43] respectively.

In reality, to the best of our knowledge, the relationship between the conformation of a single amphiphilic comb-like copolymer in a selective solvent and the molecular parameters is still lacking in academia. Borisov *et al.* proposed a scaling theory for the conformational behavior of comb-like copolymer in dilute solution, and revealed the existence of a transition from the pearl-necklace structure to unimolecular cylindrical and spherical micelles upon a decrease in the solvent quality for the backbone,[44] which is demonstrated by Monte Carlo and molecular dynamics simulations,[45,46] respectively. However, for a specific dilute solution, that is, the hydrophilic and hydrophobic properties of the backbone and side chains are fixed, the conformational characteristics of amphiphilic comb-like copolymers remain unclear when the molecular parameters are adjusted.

In this work, we study the conformation of amphiphilic comb-like copolymers in dilute solution using Brownian dynamics (BD) simulations. As shown in Fig. 1(a), we use a coarse-grained model in the present work, which is most commonly used in previous studies.[26,27,30,32,47,48] An amphiphilic comb-like chain is modeled as a bead-spring chain consisting of N_b hydrophobic backbone beads (red) and N_g hydrophilic beads for one side chain (green), and for simplicity, it is assumed that the side chains are uniformly grafted onto the backbone. The grafting density (σ_s) is defined as $\sigma_s = 1/N_s$, where N_s denotes the degree of polymerization between two neighboring grafting points. Adjacent beads in the backbone and side chains, and the grafting point between the bead of side chains and the bead of backbone, are connected by the finitely extension nonlinear elastic (FENE) potential,[49] $U_{FENE}(r) = -0.5\kappa R_0^2 \ln[1-(r/R_0)^2]$, where κ denote the spring constant and R_0 is the maximum separation distance for the bead-bead distance r. The nonbonded interaction between two beads accounted for the excluded-volume interaction is described through the Lennard-Jones (LJ) potential,[50] $U_{LJ}(r) = 4\varepsilon[(\sigma/r)^{12} - (\sigma/r)^6]$, where ε and σ denotes the energy and length parameters, respectively. For the interaction between hydrophobic beads, we set the cutoff of the LJ potential to be $r_c = 2.5\sigma$, which corresponds to the poor solvent condition.[51,52] While for other pairwise interactions, including between hydrophilic beads and between hydrophobic and hydrophilic beads, we only consider the purely repulsive LJ potential, also known as the WCA potential, by setting $r_c = 2^{1/6}\sigma$, which corresponds to the good solvent condition.[50] All LJ potentials are shifted so that $U_{LJ} = 0$ at r_c.

The BD equation of motion for the bead i is described by $\dot{\mathbf{r}}_i(t) = -\frac{1}{\xi}\nabla U_i + \frac{1}{\xi}\mathbf{f}_i(t)$.[53] Here U_i represents the sum of all LJ and FENE potentials discussed above, and ξ is the friction coefficient of a bead in the solvent with the viscosity η, based on the Stokes-Einstein relation, which can be written as $\xi = 6\pi\eta a$. $\mathbf{f}_i(t)$ denotes a random force related to ξ by the fluctuation dissipation theorem $\langle \mathbf{f}_i(t)\mathbf{f}_j(t')\rangle = 2\xi k_B T\delta_{ij}\delta(t-t')\mathbf{I}$, where $\mathbf{I}$ is the unit tensor. The equations are integrated with an Euler integrator, the inertia effect is ignored in this method, which allows us to compute longer time steps with less computational effort. In addition, we only focus on the conformations of amphiphilic comb-like copolymers, excluding the dynamic properties such as diffusion, thus, the intramolecular hydrodynamic interactions (HI) are not taken into account, which is a reasonable and economical choice.

We simulate the conformation of an amphiphilic comb-like chain in a cubic box with dimensions of (D, D, D), where the periodic boundary conditions are imposed along all directions. In this work, σ, m and ε are taken to be the units of length, mass and energy, respectively, and the unit of time is $\tau = (m\sigma^2/\varepsilon)^{1/2}$. We set the FENE parameters as $\kappa = 30$ and $R_0 = 1.5$, which can prevent chains crossing.[54] We fix the temperature as $k_BT = 1.0$, the time step as $\Delta t = 10^{-4}$, and the friction coefficient as $\xi = 0.5$, respectively. Moreover, the simulation box is fixed as $D = 150$. In each case, 100 samples were averaged with 2×10^8 simulation steps. We tune the grafting density from 0 to 1 ($0 \le \sigma_s \le 1$), *i.e.*, from no grafting on the backbone to each backbone bead grafting a side chain, partly shown in Fig. 1(b), where a transition from a single hydrophobic core to the formation of spherical core-shell structures to cylindrical core-shell structures is observed.

We first calculate the ratio of the radius of gyration of the amphiphilic comb-like chain and the hydrophobic backbone itself (R_g/R_{g0}) as a function of σ_s in Figs. 2(a)–2(c). When $N_b = 20$ (Fig. 2a), the results show that with the increase of σ_s, R_g/R_{g0} increases rapidly at first and then slowly, and the increase in the length of side chains would promote this transition. In reality, when σ_s is low, such as less than 0.2, the side chains outside the hydrophobic core are relatively sparse. As σ_s is increased, a spherical micelle with the core-shell structure will be formed. And thereafter, the increase in the number of side chains makes minor contribution to the size of the spherical micelle.

In order to further prove the shape of the micelle, we calculate the three eigenvalues of the radius of gyration tensor ($\lambda_3^2 \ge \lambda_2^2 \ge \lambda_1^2$) as shown in Figs. 2(d)–2(f), which corresponds to the simulation snapshots in Figs. 2(a)–2(c), respectively. The results in Fig. 2(d) show that the three eigenvalues are almost the same, which indicates that the spherical micelles with the core-shell structure are indeed formed. Then, we

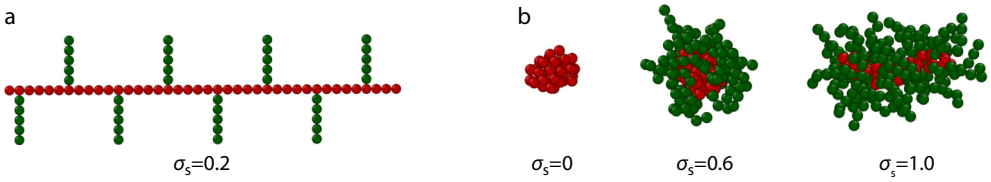

Fig. 1 (a) Model of an amphiphilic comb-like chain with the length of the hydrophobic backbone $N_b = 40$ (red), the length of the hydrophilic side chains $N_g = 5$ (green) and the grafting density $\sigma_s = 0.2$; (b) Simulation snapshots of conformations of an amphiphilic comb-like chain with $N_b = 40$ and $N_g = 5$, where σ_s is 0, 0.6 and 1, respectively.

https://doi.org/10.1007/s10118-023-2912-8

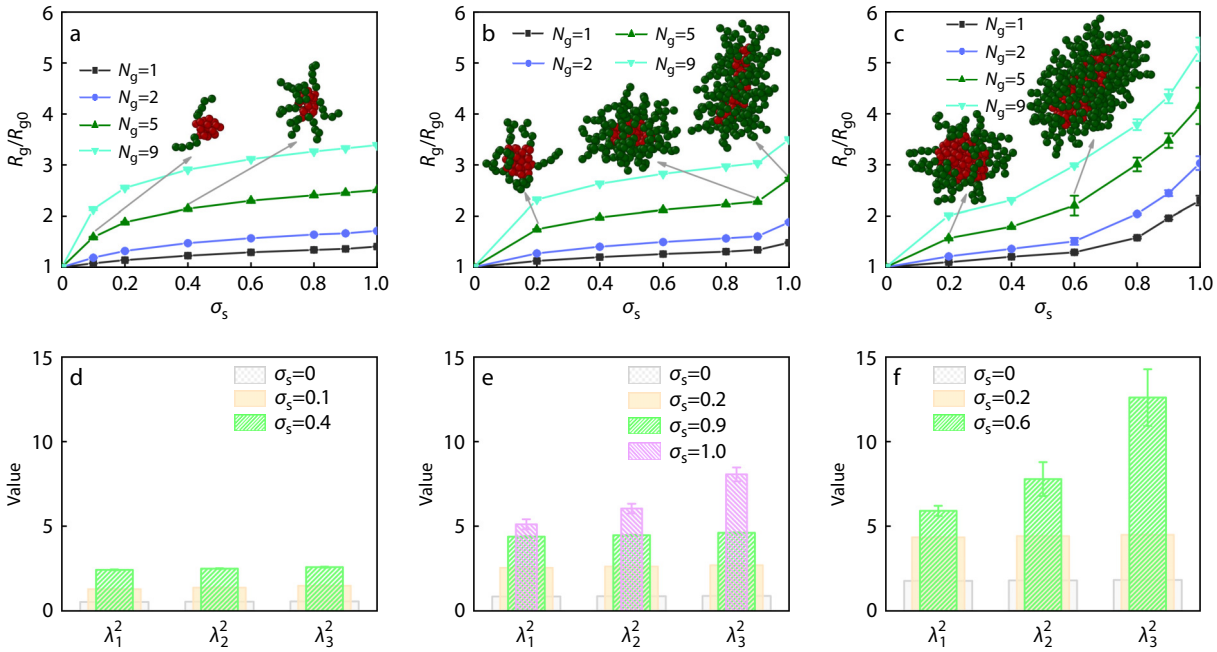

Fig. 2 (a–c) Ratio of the radius of gyration of the amphiphilic comb-like chain and the hydrophobic backbone itself (R_g/R_{g0}) as a function of the grafting density (σ_s) with $N_g = 1$, 2, 5 and 9, where (a) is $N_b = 20$, (b) is $N_b = 40$, and (c) is $N_b = 120$, respectively. The representative snapshots of simulations are also included in (a) to (c). (d–f) Three eigenvalues ($\lambda_3^2 \geq \lambda_2^2 \geq \lambda_1^2$) of the radius of gyration tensor with different grafting densities. Except $\sigma_s = 0$, the others correspond to the representative snapshots of simulations in (a) to (c), respectively.

study the case of $N_b = 40$, as shown in Fig. 2(b), which is similar to that of $N_b = 20$ in Fig. 2(a), but when $\sigma_s = 1$, a sharp increase occurs. According to the simulation snapshots, at this time, the spherical micelle is transited to the cylindrical micelle. In Fig. 2(e), when $\sigma_s = 0.2$ or 0.9, the three eigenvalues are almost the same, proving that it is a spherical structure, but when $\sigma_s = 1$, λ_3^2 is obviously larger than the other two eigenvalues, further confirming that there is a transition from spherical micelles to cylindrical micelles. Finally, when $N_b = 120$, a different situation occurs, almost showing a trend that the size of the amphiphilic comb-like chain gradually increases with the increase of σ_s, and the increase of the length of side chains leads to this phenomenon more obvious. From the simulation snapshots in Fig. 2(c) and the three eigenvalues in Fig. 2(f), it can be concluded that the transition from spherical to cylindrical occurs at a lower grafting density.

We then study the effects of N_b and N_g on the size of amphiphilic comb-like chains, respectively, as shown in Fig. S1 (in the electronic supplementary information, ESI). For N_b, when σ_s is low, such as $\sigma_s = 0.2$ or 0.4, R_g/R_{g0} decreases with the increase of N_b, which is mainly because the size of the hydrophobic core increases with the growth of the backbone, and the shell formed by the hydrophilic side chains less contribute to the overall size, leading to this downward trend. However, when σ_s is high, with the increase of N_b, it causes the transition from spherical micelles to cylindrical micelles, as shown in Figs. 2(b) and 2(c), thus leading to an inflection point, which is related to the grafting density and the length of the hydrophobic backbone. For N_g, R_g/R_{g0} monotonously increases with the increase of N_g. The determined length of backbone forms a hydrophobic core with relatively fixed size, and the increase in N_g or σ_s can increase the size of the hydrophilic shell, thus promoting the continuous increase of the overall size.

Since different molecular parameters have different effects, we further explore the relationship between the dimension and the total degree of polymerization of amphiphilic comb-like chains, which is calculated by $N_b + \sigma_s N_b N_g$. As shown in Fig. 3, we find that a transition region is about $N_b + \sigma_s N_b N_g \approx 220$. When $N_b + \sigma_s N_b N_g$ is less than 220, R_g/R_{g0} decreases with $N_b + \sigma_s N_b N_g$. It can be seen from the comparison with Fig. S1 (in ESI) that the rate at which R_g/R_{g0} decreases with $N_b + \sigma_s N_b N_g$ is obviously lower than that with

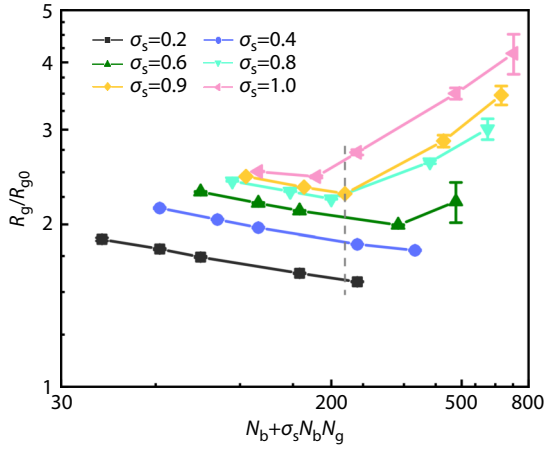

Fig. 3 Ratio of the radius of gyration of the amphiphilic comb-like chain and the hydrophobic backbone itself (R_g/R_{g0}) as a function of the total degree of polymerization of the amphiphilic comb-like chain ($N_b + \sigma_s N_b N_g$) with different grafting densities. The length of the hydrophilic side chains is fixed as $N_g = 5$.

https://doi.org/10.1007/s10118-023-2912-8

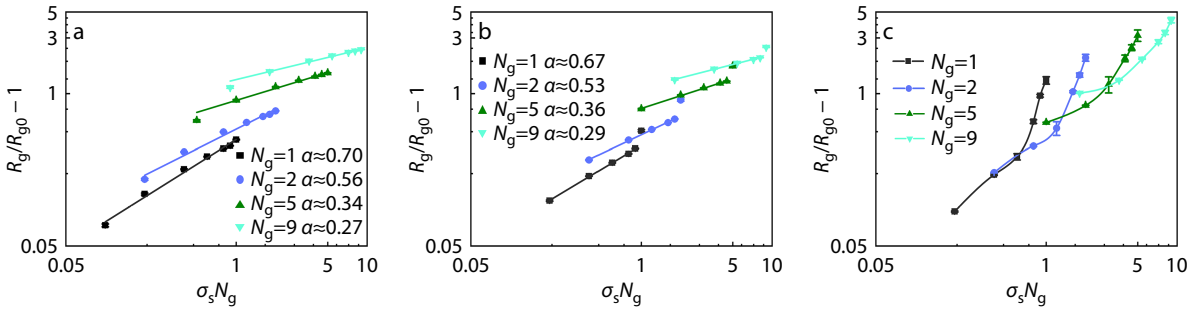

Fig. 4 Ratio of the radius of gyration of the amphiphilic comb-like chain and the hydrophobic backbone itself ($R_g/R_{g0}-1$) as a function of the stretching factor ($\sigma_s N_g$) with N_g = 1, 2, 5 and 9, where (a) is N_b = 20, (b) is N_b = 40, and (c) is N_b = 120, respectively. The data in (a) and (b, except for the last data point of each group) are fitted by $R_g/R_{g0}-1=(\sigma_s N_g)^a$, respectively.

N_b alone, which indicates that although the effect of N_b is dominant, the increase of N_g can weaken this downward trend. While when $N_b+\sigma_s N_b N_g$ is greater than 220, R_g/R_{g0} increases with the increase of $N_b+\sigma_s N_b N_g$, where N_b and N_g both play a positive role. Combining the results in Fig. 2 and a large number of simulation snapshots, we conclude that these two completely opposite regions correspond to spherical micelles and cylindrical micelles, respectively.

Theoretically, for amphiphilic block copolymers, we can predict the morphology of formed micelles by judging the competition between the interfacial energy and the conformation entropy of micelles, where always exists an optimal aggregation number to form spherical micelles. When the number of amphiphilic chains is greater than the optimal aggregation number, spherical micelles will release the conformation entropy by stretching to form cylindrical micelles or splitting to form two sub-micelles. We believe that the formation mechanism of micelles by the amphiphilic comb-like chain is similar to this, and we can thus define the optimal total degree of polymerization of the amphiphilic comb-like chain to form spherical micelles (N^*). Our results demonstrate that $N^*\approx 220$ with $N_g=5$, which is independent of N_b and σ_s. In Fig. S2 (in ESI), we display the cases of $N_g=2$ and $N_g=9$, and find N^* is about 120 and 370, respectively. Our results show that N^* increases with the length of hydrophilic side chains.

Finally, we try to use the stretching factor ($\sigma_s N_g$) to describe the conformation of amphiphilic comb-like chains, as shown in Fig. 4. When $N_b=20$ (Fig. 4a), all data points can well fall on the fitting curves, and with the increase of the length of side chains, the power exponent gradually decreases from 0.7 to 0.27. When $N_b=40$ (Fig. 4b), abnormal data points appear, that is, when $\sigma_s=1$, the data points obviously deviate from the curves formed by the lower grafting densities. Remove the last data point of each group, and the obtained power exponent decreases from 0.67 to 0.29 along with N_g from 1 to 9, which is almost consistent with the results of $N_b=20$ in (Fig. 4a). However, when $N_b=120$, we do not observe the exponential relationship, and with the increase of $\sigma_s N_g$, there will be a sudden increase, which is somewhat similar to the last point in Fig. 4(b). By comparing the results in Fig. 2, we find that the last point of each group in Fig. 4(b) and the sudden increase in Fig. 4(c) both correspond to the transition from spherical micelles to cylindrical micelles.

According to the conclusion of Fig. 3, we respectively count the changes of total degree of polymerization in Figs. 4(a)–4(c), where $24\le N_b+\sigma_s N_b N_g\le 200$ in Fig. 4(a), $48\le N_b+\sigma_s N_b N_g\le 400$ in Fig. 4(b), and $144\le N_b+\sigma_s N_b N_g\le 1200$ in Fig. 4(c), respectively. Once again, the existence of the optimal total degree of polymerization is verified, that is the total degrees of polymerization in Fig. 4(a) are always less than N^*, in Fig. 4(b), except for the last data point in each group, are also less than N^*, and while in Fig. 4(c), only the two smallest total degrees of polymerization are less than N^* and the rest are all greater than N^*. Thus, for amphiphilic comb-like chains, the stretching factor can well describe the change of chain dimensions when the total degrees of polymerization is less than N^*, which satisfies an exponential relationship and the power exponent decreases with the increase of the length of hydrophilic side chains.

In summary, the current study clearly demonstrates that, for the evaluation of dimensions of amphiphilic comb-like copolymers, there is an optimal total degree of polymerization to form spherical micelles. Only when the total degree of polymerization is less than the optimal total degree of polymerization, a unimolecular spherical micelle can be formed, otherwise, the spherical micelle will be transformed into a cylindrical micelle, which is essentially the result of the competitive balance between hydrophilic side chains and hydrophobic backbone. We further confirm that when the total degree of polymerization is less than the optimal total degree of polymerization, the radius of gyration and the stretching factor meet an exponential relationship, where the power exponent decreases with the increase of the length of hydrophilic side chains.

However, it should be pointed out that in our work, we did not observe the previously reported pearl-necklace structure.[44–46] By comparing with their model parameters, we believe that the hydrophobic interaction intensity of the backbone plays a major role. When we reduce the hydrophobic interaction intensity of the backbone, does there exist an optimal total degree of polymerization to form the pearl-necklace structure? On the other hand, the maximum ratio of the length of side chains and the length of backbone is 9/20 in this work, which means that the length of side chains is always smaller than the length of backbone. When the length of side chains further increases, even far exceeds the length of the backbone, some unexpected changes may occur. Obviously, the above issues are worthy of further exploration. In

https://doi.org/10.1007/s10118-023-2912-8

short, the fundamental principles uncovered here afford insights for the optimization of molecular design of amphiphilic comb-like copolymers in various applications.

Conflict of Interests

The authors declare no interest conflict.

Electronic Supplementary Information

Electronic supplementary information (ESI) is available free of charge in the online version of this article at http://doi.org/10.1007/s10118-023-2912-8.

ACKNOWLEDGMENTS

This work was financially supported by the Scientific Research Project of Yili Normal University (No. 2022YSYB009).

REFERENCES

1 Pan, T.; Dutta, S.; Kamble, Y.; Patel, B. B.; Wade, M. A.; Rogers, S. A.; Diao, Y.; Guironnet, D.; Sing, C. E. Materials design of highly branched bottlebrush polymers at the intersection of modeling, synthesis, processing, and characterization. *Chem. Mater.* **2022**, *34*, 1990–2024.
2 Li, Z.; Tang, M.; Liang, S.; Zhang, M.; Biesold, G. M.; He, Y.; Hao, S. M.; Choi, W.; Liu, Y.; Peng, J. Bottlebrush polymers: from controlled synthesis, self-assembly, properties to applications. *Prog. Polym. Sci.* **2021**, *116*, 101387.
3 Mohammadi, E.; Joshi, S. Y.; Deshmukh, S. A. A review of computational studies of bottlebrush polymers. *Comp. Mater. Sci.* **2021**, *199*, 110720.
4 Zhao, B. Shape-changing bottlebrush polymers. *J. Phys. Chem. B* **2021**, *125*, 6373–6389.
5 Xie, G.; Martinez, M. R.; Olszewski, M.; Sheiko, S. S.; Matyjaszewski, K. Molecular bottlebrushes as novel materials. *Biomacromolecules* **2019**, *20*, 27–54.
6 Verduzco, R.; Li, X.; Pesek, S. L.; Stein, G. E. Structure, function, self-assembly, and applications of bottlebrush copolymers. *Chem. Soc. Rev.* **2015**, *44*, 2405–2420.
7 Sheiko, S. S.; Sumerlin, B. S.; Matyjaszewski, K. Cylindrical molecular brushes: synthesis, characterization, and properties. *Prog. Polym. Sci.* **2008**, *33*, 759–785.
8 Johnson, J. A.; Lu, Y. Y.; Burts, A. O.; Lim, Y. H.; Finn, M. G.; Koberstein, J. T.; Turro, N. J.; Tirrell, D. A.; Grubbs, R. H. Core-clickable PEG-branch-azide bivalent-bottle-brush polymers by ROMP: grafting-through and clicking-to. *J. Am. Chem. Soc.* **2011**, *133*, 559–566.
9 Watanabe, M.; Mizukami, K. Well-ordered wrinkling patterns on chemically oxidized poly(dimethylsiloxane) surfaces. *Macromolecules* **2012**, *45*, 7128–7134.
10 Seong, H. G.; Chen, Z.; Emrick, T.; Russell, T. P. Reconfiguration and reorganization of bottlebrush polymer surfactants. *Angew. Chem. Int. Ed.* **2022**, *61*, e202200530.
11 Li, M.; Li, G. L.; Zhang, Z.; Li, J.; Neoh, K. G.; Kang, E. T. Self-assembly of pH-responsive and fluorescent comb-like amphiphilic copolymers in aqueous media. *Polymer* **2010**, *51*, 3377–3386.
12 Li, X.; ShamsiJazeyi, H.; Pesek, S. L.; Agrawal, A.; Hammouda, B.; Verduzco, R. Thermoresponsive PNIPAAM bottlebrush polymers with tailored side-chain length and end-group structure. *Soft Matter* **2014**, *10*, 2008–2015.
13 Pesek, S. L.; Lin, Y. H.; Mah, H. Z.; Kasper, W.; Chen, B.; Rohde, B. J.; Robertson, M. L.; Stein, G. E.; Verduzco, R. Synthesis of bottlebrush copolymers based on poly(dimethylsiloxane) for surface active additives. *Polymer* **2016**, *98*, 495–504.
14 Unsal, H.; Onbulak, S.; Calik, F.; Er-Rafik, M.; Schmutz, M.; Sanyal, A.; Rzayev, J. Interplay between molecular packing, drug loading, and core cross-Linking in bottlebrush copolymer micelles. *Macromolecules* **2017**, *50*, 1342–1352.
15 Burts, A. O.; Li, Y.; Zhukhovitskiy, A. V.; Patel, P. R.; Grubbs, R. H.; Ottaviani, M. F.; Turro, N. J.; Johnson, J. A. Using EPR To compare PEG-branch-nitroxide "bivalent-brush polymers" and traditional PEG bottle-brush polymers: branching makes a difference. *Macromolecules* **2012**, *45*, 8310–8318.
16 Li, Z.; Ma, J.; Cheng, C.; Zhang, K.; Wooley, K. L. Synthesis of hetero-grafted amphiphilic diblock molecular brushes and their self-assembly in aqueous medium. *Macromolecules* **2010**, *43*, 1182–1184.
17 Li, X.; Prukop, S. L.; Biswal, S. L.; Verduzco, R. Surface properties of bottlebrush polymer thin films. *Macromolecules* **2012**, *45*, 7118–7127.
18 Fredrickson, G. H. Surfactant-induced lyotropic behavior of flexible polymer solutions. *Macromolecules* **1993**, *26*, 2825–2831.
19 Rouault, Y.; Borisov, O. V. Comb-branched polymers: Monte Carlo simulation and scaling. *Macromolecules* **1996**, *29*, 2605–2611.
20 Feuz, L.; Leermakers, F. A. M.; Textor, M.; Borisov, O. Bending rigidity and induced persistence length of molecular bottle brushes: a self-consistent-field theory. *Macromolecules* **2005**, *38*, 8891–8901.
21 Zhang, B.; Gröhn, F.; Pedersen, J. S.; Fischer, K.; Schmidt, M. Conformation of cylindrical brushes in solution: effect of side chain length. *Macromolecules* **2006**, *39*, 8440–8450.
22 Liang, H.; Cao, Z.; Wang, Z.; Sheiko, S. S.; Dobrynin, A. V. Combs and bottlebrushes in a melt. *Macromolecules* **2017**, *50*, 3430–3437.
23 Dutta, S.; Pan, T.; Sing, C. E. Bridging simulation length scales of bottlebrush polymers using a wormlike cylinder model. *Macromolecules* **2019**, *52*, 4858–4874.
24 Dutta, S.; Sing, C. E. Two stretching regimes in the elasticity of bottlebrush polymers. *Macromolecules* **2020**, *53*, 6946–6955.
25 Morozova, S.; Lodge, T. P. Conformation of Methylcellulose as a function of poly(ethylene glycol) graft density. *ACS Macro Lett.* **2017**, *6*, 1274–1279.
26 Yethiraj, A. A Monte Carlo simulation study of branched polymers. *J. Chem. Phys.* **2006**, *125*, 204901.
27 Hsu, H. P.; Paul, W.; Rathgeber, S.; Binder, K. Characteristic length scales and radial monomer density profiles of molecular bottle-brushes: simulation and experiment. *Macromolecules* **2010**, *43*, 1592–1601.
28 Theodorakis, P. E.; Hsu, H. P.; Paul, W.; Binder, K. Computer simulation of bottle-brush polymers with flexible backbone: good solvent versus theta solvent conditions. *J. Chem. Phys.* **2011**, *135*, 164903.
29 Chatterjee, D.; Vilgis, T. A. Scaling laws of bottle-brush polymers in dilute solutions. *Macromol. Theory Simul.* **2016**, *25*, 518–523.
30 Dutta, S.; Wade, M. A.; Walsh, D. J.; Guironnet, D.; Rogers, S. A.; Sing, C. E. Dilute solution structure of bottlebrush polymers. *Soft Matter* **2019**, *15*, 2928–2941.
31 Pan, T.; Dutta, S.; Sing, C. E. Interaction potential for coarse-grained models of bottlebrush polymers. *J. Chem. Phys.* **2022**, *156*, 014903.
32 Bejagam, K. K.; Singh, S. K.; Ahn, R.; Deshmukh, S. A. Unraveling the conformations of backbone and side chains in thermosensitive bottlebrush polymers. *Macromolecules* **2019**, *52*,

9398–9408.
33 Patel, S. F.; Young, C. D.; Sing, C. E.; Schroeder, C. M. Nonmonotonic dependence of comb polymer relaxation on branch density in semidilute solutions of linear polymers. *Phys. Rev. Fluids* **2020**, *5*, 121301.
34 Mai, D. J.; Saadat, A.; Khomami, B.; Schroeder, C. M. Stretching dynamics of single comb polymers in extensional flow. *Macromolecules* **2018**, *51*, 1507–1517.
35 Mai, D. J.; Marciel, A. B.; Sing, C. E.; Schroeder, C. M. Topology-controlled relaxation dynamics of single branched polymers. *ACS Macro Lett.* **2015**, *4*, 446–452.
36 Morozova, S.; Schmidt, P. W.; Bates, F. S.; Lodge, T. P. Effect of poly(ethylene glycol) grafting density on methylcellulose fibril formation. *Macromolecules* **2018**, *51*, 9413–9421.
37 Pan, X.; Ishaq, M. W.; Umair, A.; Ali, M. W.; Li, L. Evolution of single chain conformation for model comb-like chains with grafting density ranging from 0 to 100% in dilute solution. *ACS Macro Lett.* **2019**, *8*, 1535–1540.
38 Pan, X.; Ding, M.; Li, L. Experimental validation on average conformation of a comblike polystyrene library in dilute solutions: universal scaling laws and abnormal SEC elution behavior. *Macromolecules* **2021**, *54*, 11019–11031.
39 Pan, X.; Ishaq, M. W.; Ali, M. W.; Yang, J.; Li, L.; Chen, Y. Unraveling the conformational properties of comb-like poly(propargyl acrylate)-graft-poly(2-ethyl-2-oxazoline) chains in dilute solutions. *Polymer* **2021**, *233*, 124224.
40 Tang, Z.; Pan, X.; Zhou, H.; Li, L.; Ding, M. Conformation of a comb-like chain free in solution and confined in a nanochannel: from linear to bottlebrush structure. *Macromolecules* **2022**, *55*, 8668–8675.
41 Qiu, X. Y.; Jiang, M. W.; Guo, C. G.; He, Y. J.; Wang, C. Q. Self-assembled nano-wire of an amphiphilic biodegradable oligosaccharide-based graft copolymer in water. *Carbohyd. Polym.* **2012**, *87*, 2306–2312.
42 Chang, H. Y.; Lin, Y. L.; Sheng, Y. J.; Tsao, H. K. Structural characteristics and fusion pathways of onion-like multilayered polymersome formed by amphiphilic comb-like graft copolymers. *Macromolecules* **2013**, *46*, 5644–5656.
43 Liu, Y. T.; Li, Y. R.; Wang, X. Spontaneous onion shape vesicle formation and fusion of comb-like block copolymers studied by dissipative particle dynamics. *RSC Adv.* **2017**, *7*, 5130–5135.
44 Borisov, O. V.; Zhulina, E. B. Amphiphilic graft copolymer in a selective solvent: intramolecular structures and conformational transitions. *Macromolecules* **2005**, *38*, 2506–2514.
45 Košovan, P.; Kuldová, J.; Limpouchová, Z.; Procházka, K.; Zhulina, E. B.; Borisov, O. V. Amphiphilic graft copolymers in selective solvents: molecular dynamics simulations and scaling theory. *Macromolecules* **2009**, *42*, 6748–6760.
46 Kramarenko, E. Y.; Pevnaya, O. S.; Khokhlov, A. R. Stoichiometric polyelectrolyte complexes as comb copolymers. *J. Chem. Phys.* **2005**, *122*, 084902.
47 Lyubimov, I.; Wessels, M. G.; Jayaraman, A. Molecular dynamics simulation and prism theory study of assembly in solutions of amphiphilic bottlebrush block copolymers. *Macromolecules* **2018**, *51*, 7586–7599.
48 Wessels, M. G.; Jayaraman, A. Molecular dynamics simulation study of linear, bottlebrush, and star-like amphiphilic block polymer assembly in solution. *Soft Matter* **2019**, *15*, 3987–3998.
49 Kremer, K.; Grest, G. S. Dynamics of entangled linear polymer melts: a molecular-dynamics simulation. *J. Chem. Phys.* **1990**, *92*, 5057–5086.
50 Weeks, J. D.; Chandler, D.; Andersen, H. C. Role of repulsive forces in determining the equilibrium structure of simple liquids. *J. Chem. Phys.* **1971**, *54*, 5237–5247.
51 Reddy, G.; Yethiraj, A. Implicit and explicit solvent models for the simulation of dilute polymer solutions. *Macromolecules* **2006**, *39*, 8536–8542.
52 Ding, M.; Chen, Q.; Duan, X.; Shi, T. Flow-driven translocation of a diblock copolymer through a nanopore. *J. Phys. Chem. B* **2019**, *123*, 8848–8852.
53 Ermak, D. L.; McCammon, J. A. Brownian dynamics with hydrodynamic interactions. *J. Chem. Phys.* **1978**, *69*, 1352–1360.
54 Kumar, S.; Larson, R. G. Brownian dynamics simulations of flexible polymers with spring–spring repulsions. *J. Chem. Phys.* **2001**, *114*, 6937–6941.

https://doi.org/10.1007/s10118-023-2912-8